Interactions and Stress Relaxation in Monolayers of Soft Nanoparticles at Fluid-Fluid Interfaces

Valeria Garbin*
Department of Chemical Engineering, Imperial College London, London SW7 2AZ, United Kingdom

Ian Jenkins, Talid Sinno, John C. Crocker, and Kathleen J. Stebe
Department of Chemical and Biomolecular Engineering, University of Pennsylvania, 220 South 33rd Street, Philadelphia, Pennsylvania 19104, USA

(Received 5 October 2014; revised manuscript received 19 January 2015; published 9 March 2015)

Nanoparticles with grafted layers of ligand molecules behave as soft colloids when they adsorb at fluid-fluid interfaces. The ligand brush can deform and reconfigure, adopting a lens-shaped configuration at the interface. This behavior strongly affects the interactions between soft nanoparticles at fluid-fluid interfaces, which have proven challenging to probe experimentally. We measure the surface pressure for a stable 2D interfacial suspension of nanoparticles grafted with ligands, and extract the interaction potential from these data by comparison to Brownian dynamics simulations. A soft repulsive potential with an exponential form accurately reproduces the measured surface pressure data. A more realistic interaction potential model is also fitted to the data to provide insights into the ligand configuration at the interface. The stress of the 2D interfacial suspension upon step compression exhibits a single relaxation time scale, which is also attributable to ligand reconfiguration.

DOI: 10.1103/PhysRevLett.114.108301 PACS numbers: 82.70.Dd, 83.50.Lh

Soft colloids at fluid-fluid interfaces, for instance star copolymers [1], microgels [2,3], and polymer- or ligand-grafted nanoparticles [4–9], stretch and deform, adopting shapes that are dictated by the interplay of surface tension and deformability, much like in the wetting of membranes, vesicles [10], and soft solids [11,12]. Ligand-grafted metal or semiconductor nanocrystals at fluid-fluid interfaces are widely used in nanomaterials synthesis [13–15] and in catalytic processes [16]. Simulation studies predict the rearrangement of the ligand brush into anisotropic lens-shaped configurations when these nanoparticles adsorb at fluid-fluid interfaces [4–6,8]. This prediction is supported by x-ray reflectivity measurements of nanoparticle density at the interface [7]. These configurations are particularly important, as ligand rearrangements modify the interparticle interactions, which ultimately determine colloidal stability and phase behavior at the interface. Ligand-mediated interactions can be dominant in the case of soft nanoparticles, where the thickness of the deformable grafted layer is comparable to the size of the particle core. These interactions have been studied in simulations [9] but have never been characterized experimentally. Direct measurements of the interparticle potential have been hampered by the challenge of obtaining a stable nanoparticle suspension at a fluid-fluid interface. Specifically, since adsorption at the interface exposes the nanoparticles to a second fluid with different polarity and solvent quality, colloidal stability is not always preserved [17].

Here we report measurements of the steric repulsion between ligand-grafted nanoparticles, with a length of the ligand comparable to the radius of the nanoparticle, within a fluid-fluid interface (see Fig. 1). We measured the surface pressure of a 2D nanoparticle suspension as a function of surface coverage, and related it to an effective pair potential using Brownian dynamics simulations. A soft repulsive potential with exponential decay accurately captures the measured surface pressure. An empirical interaction potential is also fitted to the data to provide insights into the ligand configuration. In a step-compression experiment we find a slow relaxation time scale, which we conclude is due to slow rearrangements of the ligands grafted on the surface of the nanoparticles, resulting in a time-dependent interaction potential.

The nanoparticles used for the experiments are 4.5 nm gold nanocrystals grafted with an amphiphilic ligand, mercapto-undecyl-tetra(ethylene glycol). The particle polydispersity, estimated from a transmission electron micrograph provided by the supplier (Sigma-Aldrich), is at

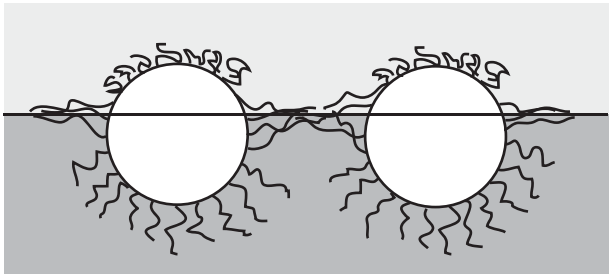

FIG. 1. Schematic of nanoparticles at fluid-fluid interface with ligand rearrangements (drawing not to scale).

least 10%. These particles exhibit spontaneous adsorption from an aqueous suspension onto the interface with fluorinated oil octafluoropentyl acrylate [18]. The oil was obtained from Sigma-Aldrich and used as received. The surface tension of the bare oil-water interface is $\gamma_0 = 26$ mN/m. Adsorption of the nanoparticles at the oil-water interface effectively reduces the surface tension [18]. We measured the effective surface tension by pendant drop tensiometry. Briefly, the shape of a pendant drop is determined by the balance of surface tension and gravitational forces, described by the Bond number $\mathrm{Bo} = \Delta\rho g R^2/\gamma$ where $\Delta\rho$ is the density difference and γ the surface tension between the two fluids, g the acceleration due to gravity, and R the radius of the drop. A numerical solution to the Young-Laplace equation is fitted to the contour of the drop to extract the surface tension.

In general, the effective surface tension is given by $\gamma = \gamma_0 - \Pi$ where Π is the two-dimensional osmotic pressure, referred to as surface pressure, due to the interfacial nanoparticles. If the interfacial phase is a stable suspension, and in the absence of extra stresses due to dynamic deformation, the measured pressure Π_0 is an equilibrium property of the suspension that only depends on the nanoparticle surface coverage ϕ. Upon dynamic deformation, transient stresses can arise due to nonequilibrium configurations of the interfacial nanoparticles or of the grafted ligand layers, which subsequently relax when the system has reached a new equilibrium configuration. We probed the relaxation time scales of the system by performing compression experiments at different strain rates and step-compression experiments. One of the limitations of pendant drop tensiometry for these measurements is that the Young-Laplace equation is fitted to the shape of a dynamically deforming drop. This approach is justified if viscous and inertial stresses in the bulk are negligible compared with surface stresses [19]. The capillary number and the Weber number during our step-compression experiments are both small ($\mathrm{Ca} = (\eta\dot{R}/\gamma) \approx 10^{-5}$, $\mathrm{We} = (\rho\dot{R}^2 R/\gamma) \approx 10^{-7}$) confirming that surface stresses are dominant.

We previously reported surface pressure measurements revealing that this nanoparticle system forms a stable 2D suspension over a broad range of surface coverages [20]. The nanoparticle surface coverage $\phi = N\pi a^2/A$, expressed in terms of the hard-core radius a of the particles, was obtained from optical absorbance measurements as described in our previous work. We also found that beyond a critical surface pressure $\Pi_c \approx 13$ mN/m, the short-range, ligand-mediated repulsive interactions promote expulsion of the particles out of the interface and back into the bulk suspension. In contrast, cohesive nanoparticle monolayers buckle like elastic films upon compression [21]. This observation further confirms that, in the entire range of surface pressures considered here, $\Pi \sim 0$–10 mN/m, the interfacial layer of nanoparticles remains fluid and its elasticity is negligible.

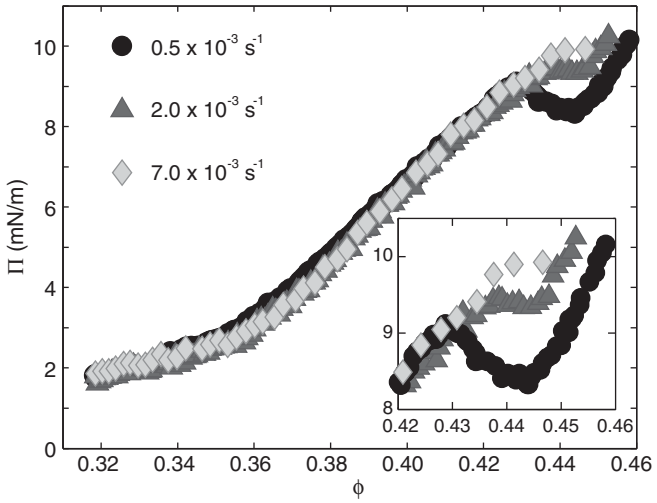

FIG. 2. Surface pressure as a function of surface coverage for three values of interfacial dilatational strain rate. The surface pressure is independent of the rate of compression up to $\phi \approx 0.43$. Rate-dependent behavior is observed for $\phi > 0.43$ (see inset), and discussed in the text.

Figure 2 shows the surface pressure as a function of surface coverage for three values of the interfacial dilatational strain rate $\dot{\alpha} = (1/A)(dA/dt)$. By preparing the interface with a fixed number of particles N and changing the area A of the drop at constant N, we measured the surface pressure as a function of surface coverage. In practice, we performed compression experiments at sufficiently high initial surface coverage and sufficiently low volume fraction that the rate of change of surface pressure due to adsorption from the bulk (10^{-4} mN m^{-1} s^{-1}, see [20]) is much lower than the strain rate, therefore ensuring that N can be considered constant. The strain rate $\dot{\alpha}$ was kept sufficiently small that the monolayer could equilibrate upon compression, as will be discussed below. Up to a surface coverage $\phi \approx 0.43$, where $\Pi \approx 9$ mN/m, the response is independent of $\dot{\alpha}$ (see Fig. 2) and reversible upon expansion (as shown in [20]), to within the limits of experimental repeatability. Because the surface viscosity of the interfacial suspension increases with ϕ, the reversibility of the compression isotherm over the whole range $0.32 < \phi < 0.43$ indicates that interfacial viscous stresses relax on time scales faster than the time scale of the fastest compression rate, of the order of 10^{-2} s^{-1}.

To extract the effective interaction potential, we performed canonical ensemble 2D Brownian dynamics simulations using a short-range soft repulsive force of the form $F(r) = F_0 \exp[-(r - 2a)/\lambda]$. The surface pressure Π_0 was computed for particle coverages in the range $0.33 \leq \phi \leq 0.45$. The van der Waals force between gold cores is estimated to be 10 times smaller than the magnitude of the ligand-mediated repulsion in the range of separation distances considered, and so was not included in the force field. The prefactor F_0 and decay length λ are determined

by least-squares regression of the computed osmotic pressure Π_0 to the experimental data collected with the slowest strain rate. The stated errors in all parameters reflect the combined effect of fitting uncertainties and experimental calibration uncertainties. In simulation, the particles are monodisperse and the system favors crystalline order for surface coverage $\phi > 0.30$. By initializing the system in a disordered state and a crystalline state at $\phi = 0.30$ the resulting osmotic pressures were found to be the same to within 2%, suggesting that the polydispersity of the particles in the experiment (which may suppress crystallization) does not significantly affect the osmotic pressure. Simulation studies of nanoparticle adsorption kinetics also confirm that the surface pressure is unaffected by polydispersity [8]. A single set of parameters is found, $F_0 = (6 \pm 3) \times 10^{-16}$ N and $\lambda = (0.60 \pm 0.02)$ nm, that gives the best fit to the experimental data as shown in Fig. 3(a). Figure 3(b) is the fitting surface for this force field, displaying the sums of the squares of the residuals. The short-ranged soft potential is also in qualitative agreement with the results of numerical simulations of the mean-field potential between polymer-grafted nanoparticles at fluid-fluid interfaces [9].

A frequently used interaction potential model for steric repulsion is the Alexander-de Gennes (AdG) model, which relates the interaction strength to molecular details.

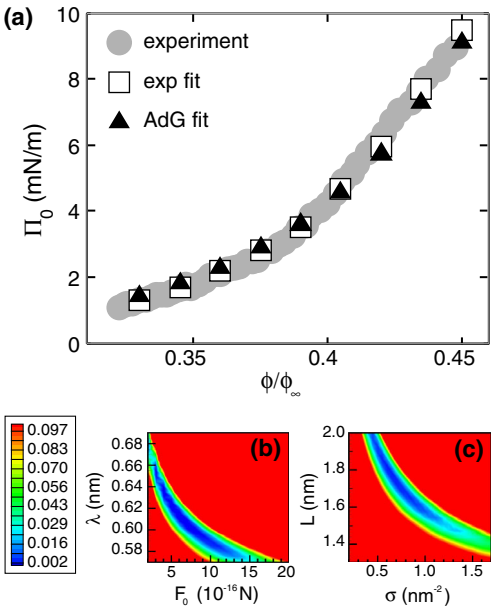

FIG. 3 (color online). (a) Experimentally measured osmotic pressure (filled circles). Computed surface pressure for an exponentially decaying interaction force (hollow squares) and the Alexander–de Gennes (AdG) model (filled triangles). The surface coverage ϕ is normalized by the maximum surface coverage for hard disks $\phi_\infty \approx 0.91$. (b) Fitting surface for exponential interaction force. (c) Fitting surface for Alexander–de Gennes interaction model. Color map in (b) and (c) corresponds to the sum of squares of residues (scale shown to the left).

The pressure between flat plates with grafted ligands is given by $P(h) = k_B T \sigma^{3/2}[(2L/h)^{9/4} - (h/2L)^{3/4}]$ where h is the separation distance between the plates, L is the thickness of the brush, and σ the grafting density [22]. The best fit of the surface pressure obtained with this model captures the experimental data no better than the simpler exponential form [see Fig. 3(a)] but does provide estimates for its relevant physical parameters: $L = (1.8 \pm 0.1)$ nm and $\sigma = (0.6 \pm 0.3)$ nm^{-2} [Fig. 3(c)]. The value of L can be compared with the contour length of a undecyl-tetra(ethylene glycol) molecule of approximately 2 nm, corroborating the picture that the ligands are almost completely stretched out in the plane of the interface. One limitation to the interpretability of this model is that, in deriving the interaction force between the particles, we assumed a brush of uniform thickness L over the surface of the particle. This assumption appears inconsistent with the hypothesis of ligand rearrangements at the fluid interface. However, since the steric repulsion is localized to a small contact area between the brushes, it seems plausible that the AdG model gives a measure of the local thickness of the brush in that contact area.

To more sensitively detect any time-dependent relaxation phenomena in the interfacial nanoparticle monolayer, we performed a step-compression experiment. After rapidly increasing the surface coverage from $\phi \approx 0.30$ to $\phi \approx 0.34$ (interfacial dilatational strain $\alpha = \Delta A/A_0 \approx 0.1$), we observed a time-dependent surface pressure as shown in Fig. 4. Before compression, the equilibrium surface pressure is $\Pi_0 \approx 1.45$ mN/m (solid triangle). At long times, the surface pressure plateaus to the equilibrium value corresponding to the final surface coverage after compression, $\Pi_0 \approx 2.40$ mN/m. The time-dependent difference from this final pressure can be fit to a sum of two exponentials, $\Delta\Pi(t) = \Delta\Pi_1 \exp(-t/\tau_1) + \Delta\Pi_2 \exp(-t/\tau_2)$ with

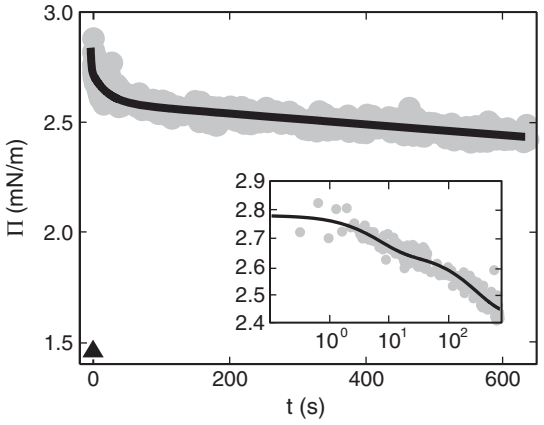

FIG. 4. Stress relaxation behavior in a step-compression experiment (solid circles). The initial surface pressure is 1.45 mN/m (solid triangle). The extra stress decays to zero with two relaxation time scales. The fast time scale ($\tau_1 = 6$ s) is due to coadsorbed ligands. The slow dynamics ($\tau_2 = 266$ s) is attributable to ligand rearrangements.

$\Delta\Pi_1 = 0.13$ mN/m, $\tau_1 = 6$ s and $\Delta\Pi_2 = 0.22$ mN/m, $\tau_2 = 266$ s. Neither a power law nor a stretched exponential capture the stress relaxation behavior, in contrast with viscoelastic monolayers of soft colloids at interfaces such as protein monolayers, which have relaxation following a stretched exponential decay [23]. The nonuniform rate of change of area over the surface of a pendant drop results in gradients in surface coverage, which could produce unaccounted for Marangoni stresses. These stresses do not affect the measurement if the time scale of the convective flow that relaxes the gradient in surface coverage, $\tau_M = \eta R/\Delta\gamma$, is sufficiently fast [24,25]. The maximum difference in surface tension over the surface of the drop can be estimated as the change in surface tension upon compression, $\Delta\gamma \approx 1$ mN/m. The time scale of the Marangoni flow is then $\tau_M \approx 10^{-3}$ s, significantly faster than the relaxation time scales observed in the experiment.

We hypothesize that the faster relaxation process ($\tau_1 = 6$ s) is due to coadsorbed free ligands [26], and that the slow dynamics are attributable to the reconfiguration of the ligands on the nanoparticles. To assess the effect of free ligands we performed control experiments with supernatant fluid obtained by centrifuging the nanoparticles. The surface tension between oil and the supernatant fluid decreases by 0.3 mN/m after a clean interface is formed, confirming the presence of traces of free ligands in solution [20]. Step-compression experiments with supernatant fluid show a single relaxation time scale comparable to the fast process seen here. The slow process, in contrast, requires the presence of the nanoparticles themselves. The observed relaxation suggests some manner of slow reconfiguration of the particle-grafted ligands at the interface, resulting in a time-dependent interaction potential and a time-dependent surface pressure $\Pi(t)$. This suggests that the faster of the quasistatic compressions in Fig. 2 could still be subject to dynamical effects, and so the interpretation of Fig. 2 as an equilibrium curve is to be treated with care. Because the two faster strain rates used were not sufficiently slow compared to the slow relaxation time ($\tau_2 = 266$ s), the corresponding data do not formally report the true equilibrium surface pressure of the system. The apparent independence of the measured surface pressure to the strain rate at coverages $\phi < 0.43$ is most likely due to the small pressure contribution of the slow relaxation process, $\Delta\Pi_2 = 0.22$ mN/m. This value can therefore be regarded as an uncertainty in the quasistatic surface pressure data presented in Fig. 2.

The surface pressure depends on the strain rate and the system displays interesting nonmonotonic behavior for coverages $\phi > 0.43$ (see inset in Fig. 2). The appearance of the effect only for sufficiently slow compression, and, in particular, at strain rates comparable to the reciprocal of the slow relaxation seen in the step compression, suggests that it may be due to the same relaxation process as in Fig. 4. At higher surface coverage $\phi > 0.43$, its amplitude has become sufficiently large to be visible also in the constant strain rate experiments. We identify two possible physical mechanisms for this effect. One possible explanation is phase separation of the binary mixture of nanoparticles and coadsorbed free ligands at the interface, which is only observed if compression is sufficiently slow that the mixture can equilibrate. Alternatively, the rate-dependent behavior can be interpreted as follows: for $\phi > 0.43$, the surface-to-surface interparticle separation ($h \approx 2.2$ nm) is comparable to the contour length of the ligands, and therefore the ligand brushes are significantly compressed. The resulting osmotic pressure within the brush, which contributes to the increase in surface pressure, means that it is entropically unfavorable for the ligands to remain in the contact area between the particles. As the ligands are free to move over the surface of the particles because the thiol-gold bond is mobile [27], the ligand brush slowly reconfigures. The slow time scale for reconfiguration is attributable to the competition between the osmotic pressure forcing the ligands away from the contact area, and the favorable configuration of the ligands lying flat on the interface (Fig. 1). As a consequence this transition is only observed for the slowest compression rate ($\dot{\alpha} = 0.5 \times 10^{-3}$ s^{-1}, circles). Ligand reconfiguration results in stress relaxation when the brushes become less compressed as the density of ligands in the contact area decreases. The increase in pressure upon compression resumes from $\phi > 0.45$, when the brushes reach their new configuration, with lower density in the contact area between the particles. For faster compression rates ($\dot{\alpha} = 5 \times 10^{-3}$ s^{-1}) this effect is less pronounced, and for the fastest compression rate ($\dot{\alpha} = 7 \times 10^{-3}$ s^{-1}) it is almost absent because the ligand brush is quenched in a configuration where the ligands cannot rearrange, and the pressure increases monotonically.

Our measurement of the interaction potential between soft nanoparticles at fluid-fluid interfaces corroborates the picture that ligands stretch out into lenslike configurations at the interface. The grafted ligand layer dominates not only interparticle interactions but also stress relaxation through ligand rearrangements and a reconfiguration of the layer. Our measurements also confirm the importance of surface-active trace ligands in the behavior of nanoparticle-laden fluid-fluid interfaces. The equilibrium behavior and mechanical response of nanoparticle monolayers have important consequences in many emerging applications that exploit nanoparticles at fluid-fluid interfaces, for instance, in the making of 2D nanomaterials with tunable optical properties [13,14] where precise control of interactions and stability is crucial for obtaining reversible properties. Our experimental method for the measurement of interactions between nanocolloids at fluid interfaces makes it possible to validate simulation studies not only of the mean-field interaction potential between ligand-coated nanoparticles [9] but also of the effect of 2D confinement on the interaction potential between star polymers [28] and other soft nanoparticles.

*v.garbin@imperial.ac.uk

[1] H. Xu, R. Erhardt, V. Abetz, A. H. E. Müller, and W. A. Goedel, Janus micelles at the air/water interface, Langmuir **17**, 6787 (2001).
[2] M. Destribats, V. Lapeyre, M. Wolfs, E. Sellier, F. Leal-Calderon, V. Ravaine, and V. Schmitt, Soft microgels as Pickering emulsion stabilisers: Role of particle deformability, Soft Matter **7**, 7689 (2011).
[3] K. Geisel, L. Isa, and W. Richtering, Unraveling the 3D localization and deformation of responsive microgels at oil/water interfaces: A step forward in understanding soft emulsion stabilizers, Langmuir **28**, 15770 (2012).
[4] K. A. Tay and F. Bresme, Wetting properties of passivated metal nanocrystals at liquid-vapor interfaces: A computer simulation study, J. Am. Chem. Soc. **128**, 14166 (2006).
[5] R. J. K. Udayana Ranatunga, R. J. B. Kalescky, C.-c. Chiu, and S. O. Nielsen, Molecular dynamics simulations of surfactant functionalized nanoparticles in the vicinity of an oil/water interface, J. Phys. Chem. C **114**, 12151 (2010).
[6] J. M. D. Lane and G. S. Grest, Spontaneous Asymmetry of Coated Spherical Nanoparticles in Solution and at Liquid-Vapor Interfaces, Phys. Rev. Lett. **104**, 235501 (2010).
[7] L. Isa, D. C. E. Calzolari, D. Pontoni, T. Gillich, A. Nelson, R. Zirbs, A. Sanchez-Ferrer, R. Mezzenga, and E. Reimhult, Core-shell nanoparticle monolayers at planar liquid-liquid interfaces: effects of polymer architecture on the interface microstructure, Soft Matter **9**, 3789 (2013).
[8] K. Schwenke, L. Isa, and E. Del Gado, Assembly of nanoparticles at liquid interfaces: crowding and ordering, Langmuir **30**, 3069 (2014).
[9] K. Schwenke, L. Isa, D. L. Cheung, and E. Del Gado, Conformations and effective interactions of polymer-coated nanoparticles at liquid interfaces, Langmuir **30**, 12578 (2014).
[10] H. Kusumaatmaja, Y. Li, R. Dimova, and R. Lipowsky, Intrinsic Contact Angle of Aqueous Phases at Membranes and Vesicles, Phys. Rev. Lett. **103**, 238103 (2009).
[11] R. Pericet-Cámara, A. Best, H.-J. Butt, and E. Bonaccurso, Effect of capillary pressure and surface tension on the deformation of elastic surfaces by sessile liquid microdrops: An experimental investigation, Langmuir **24**, 10565 (2008).
[12] A. Marchand, S. Das, J. H. Snoeijer, and B. Andreotti, Contact Angles on a Soft Solid: From Young's Law to Neumann's Law, Phys. Rev. Lett. **109**, 236101 (2012).
[13] A. Tao, P. Sinsermsuksakul, and P. Yang, Tunable plasmonic lattices of silver nanocrystals, Nat. Nanotechnol. **2**, 435 (2007).
[14] M. Luo, G. K. Olivier, and J. Frechette, Electrostatic interactions to modulate the reflective assembly of nanoparticles at the oil-water interface, Soft Matter **8**, 11923 (2012).
[15] V. A. Turek, M. P. Cecchini, J. Paget, A. R. Kucernak, A. A. Kornyshev, and J. B. Edel, Plasmonic ruler at the liquid-liquid interface, ACS Nano **6**, 7789 (2012).
[16] S. Crossley, J. Faria, M. Shen, and D. E. Resasco, Solid nanoparticles that catalyze biofuel upgrade reactions at the water/oil interface, Science **327**, 68 (2010).
[17] V. Garbin, J. C. Crocker, and K. J. Stebe, Nanoparticles at fluid interfaces: Exploiting capping ligands to control adsorption, stability and dynamics, J. Colloid Interface Sci. **387**, 1 (2012).
[18] K. Du, E. Glogowski, T. Emrick, T. P. Russell, and A. D. Dinsmore, Adsorption energy of nano- and microparticles at liquid-liquid interfaces, Langmuir **26**, 12518 (2010).
[19] L. M. C. Sagis, Dynamic properties of interfaces in soft matter: Experiments and theory, Rev. Mod. Phys. **83**, 1367 (2011).
[20] V. Garbin, J. C. Crocker, and K. J. Stebe, Forced desorption of nanoparticles from an oil-water interface, Langmuir **28**, 1663 (2012).
[21] S. S. Datta, H. C. Shum, and D. A. Weitz, Controlled buckling and crumpling of nanoparticle-coated droplets, Langmuir **26**, 18612 (2010).
[22] P.-G. de Gennes, Polymers at an interface; a simplified view, Adv. Colloid Interface Sci. **27**, 189 (1987).
[23] P. Cicuta, Compression and shear surface rheology in spread layers of β-casein and β-lactoglobulin, J. Colloid Interface Sci. **308**, 93 (2007).
[24] H. Wong, D. Rumschitzki, and C. Maldarelli, Marangoni effects on the motion of an expanding or contracting bubble pinned at a submerged tube tip, J. Fluid Mech. **379**, 279 (1999).
[25] D. Tam, V. von Arnim, G. H. McKinley, and A. E. Hosoi, Marangoni convection in droplets on superhydrophobic surfaces, J. Fluid Mech. **624**, 101 (2009).
[26] J. van Rijssel, M. van der Linden, J. D. Meeldijk, R. J. A. van Dijk-Moes, A. P. Philipse, and B. H. Erné, Spatial Distribution of Nanocrystals Imaged at the Liquid-Air Interface, Phys. Rev. Lett. **111**, 108302 (2013).
[27] C. Vericat, M. E. Vela, and R. C. Salvarezza, Self-assembled monolayers of alkanethiols on Au(111): surface structures, defects and dynamics, Phys. Chem. Chem. Phys. **7**, 3258 (2005).
[28] S. A. Egorov, J. Paturej, C. N. Likos, and A. Milchev, Controlling the interactions between soft colloids via surface adsorption, Macromolecules **46**, 3648 (2013).